Progress in Physics of Applied Materials 7 (2027), Serial Number 15, 17-30

Semnan University

Progress in Physics of Applied Materials

journal homepage: https://ppam.semnan.ac.ir/

Mechanical Strengthening Enhancement in PMMA/MWCNT/Co_3O_4 Hybrid Nanocomposites: A Comprehensive Study of Compression, Hardness, and Microstructural Properties

Noor H. Majeed, Ali K. Hattab, Ahmed A. Thamer, Reem Hussein Abdullah

College of Science, Department of Physics, Wasit University, Wasit, Iraq

ARTICLE INFO

Article history:
Received: 15 May 2026
Revised: 26 July 2026
Accepted: 20 August 2026
Published online: 15 September 2026

Keywords:
PMMA;
Multi-walled carbon nanotubes;
Cobalt oxide;
Hybrid nanocomposites;
Compression testing;
Hardness;
EDX analysis.

ABSTRACT

Hybrid nanocomposites of poly(methyl methacrylate) (PMMA) and multi-walled carbon nanotubes (MWCNTs) with cobalt oxide (Co_3O_4) nanoparticles were synthesized and systematically characterized in terms of their mechanical and microstructural properties. The nanocomposites were fabricated by a hand lay-up molding route with equal weight fractions (total loading ranging from 0.5 to 3.0 wt%) of the two nanofillers. Comprehensive characterization was carried out using compression testing (ASTM D695-15), Shore D hardness testing (ASTM D2240), X-ray diffraction (XRD), field-emission scanning electron microscopy (FE-SEM), and energy-dispersive X-ray spectroscopy (EDS/EDX). One-way analysis of variance (ANOVA) was applied to evaluate the statistical significance of the variations in the measured properties. The mechanical properties gradually improved with increasing filler concentration up to 2.0 wt% (1.0 wt% MWCNT + 1.0 wt% Co_3O_4); a further increase in filler concentration led to a deterioration in mechanical properties due to nanoparticle agglomeration. At the optimum composition, the compressive strength increased by 31.3% (from 85.6 ± 2.8 to 112.4 ± 3.2 MPa), the compressive modulus by 29.1% (from 2.85 ± 0.12 to 3.68 ± 0.15 GPa), and the Shore D hardness by 11.3% (from 82.5 ± 1.2 to 91.8 ± 1.0). All of these improvements were statistically significant ($p < 0.05$). The incorporation of cobalt and the reasonably uniform elemental distribution at lower loadings and increasing heterogeneity at higher filler content has been confirmed by the EDX point analysis and elemental mapping. The improvement is said to be due to the efficient load transfer along the MWCNTs, and to the Co_3O_4 nanoparticles, which are thought to inhibit re-agglomeration of the nanotubes, but since samples with one filler only were not prepared, the inferred synergistic effect is presented as a hypothesis. The results show that PMMA/MWCNT/Co_3O_4 hybrid nanocomposites are an interesting material for structural and protective-coating applications where high mechanical properties are required.

1. Introduction

Hybrid nanocomposites are a rapidly emerging class of materials developed by the incorporation of inorganic nanoparticles into a macroscopic organic framework [1]. The electrical, thermal, optical, dielectric, and mechanical properties, such as stiffness and strength, are significantly improved in these materials primarily due to the presence of an extensive interfacial interphase between the nanofillers and the polymer matrix [2]. This high-surface-area interfacial region plays a critical role in determining the overall performance of the composite material. Poly(methyl methacrylate) (PMMA) is a promising polymer for nanocomposite applications owing to its excellent

* Corresponding author.
E-mail address: noorhm900@uowasit.edu.iq

Cite this article as:

Majeed, N.H., Hattab, A.K., Thamer, A.A. and Abdullah, R.H., 2027. Mechanical Strengthening Enhancement in PMMA/MWCNT/Co_3O_4 Hybrid Nanocomposites: A Comprehensive Study of Compression, Hardness, and Microstructural Properties. *Progress in Physics of Applied Materials*, *7*(2),pp.17-30. DOI: **10.22075/ppam.2026.41215.1228**

optical clarity, low density, weather resistance, and mechanical stiffness [3,4]. PMMA is a biocompatible, non-toxic thermoplastic widely used in biomedical devices, optical components, and protective coatings [5,6]. Despite these desirable features, neat PMMA exhibits relatively modest mechanical strength, significant polymerization shrinkage, and moisture absorption tendency, which restrict its use in high-performance structural applications [7,8]. For this reason, extensive research has focused on enhancing the mechanical properties of PMMA through the addition of various nanofillers, including carbon nanotubes, graphene, and metal-oxide nanoparticles such as TiO_2, ZnO, and Al_2O_3 [9].

The potential for MWCNTs to be used as a reinforcement to polymer matrices is enormous because of their superior mechanical properties with tensile strengths of up to 100 GPa and elastic moduli of up to 1 TPa [10]. The quasi one-dimensional tubular nanostructure of the MWCNTs has also rendered them as a promising material for the production of multifunctional nanocomposites, because of the excellent electrical and thermal conductivity of graphene [11]. The uniform dispersion of MWCNTs in polymer matrices, however, is still a great challenge, since MWCNTs have a high tendency to self-aggregate via van der Waals interactions [12].

Cobalt Oxide Co_3O_4, a normal spinel type oxide of cobalt (II, III) is a p-type semiconductor and has a band gap of ~1.6-2.2 eV [13]. The Co_3O_4 nanostructures are promising for use in sensor, catalysis and energy storage applications due to their high specific surface area, electrochemical stability and catalytic activity [14]. Nanoparticles of Co_3O_4 when incorporated in a polymer matrix serve as rigid inclusions which facilitate load transfer between the nanofillers and the polymer matrix, resulting in reinforcement of the structure. The hybrid nanofillers comprising a combination of MWCNTs and Co_3O_4 nanoparticles are a promising solution for overcoming the disadvantages of using a single nanofiller [15]. The 0D nanoparticles can fill the gap between particles and between the particle and the matrix to increase the load transfer between particles and between the particle and the matrix, whereas the 1D MWCNTs can transfer load along the tube axis [16]. In addition, MWCNTs can also be coupled with metal-oxide nanoparticles that can prevent the aggregation of the MWCNTs and improve the dispersion and the interfacial bonding [17].

The aim of this study is to systematically explore the mechanical and microstructural properties of PMMA/MWCNT/Co_3O_4 hybrid nanocomposites. The specific objectives are: (1) fabrication of hybrid nanocomposites with a series of different MWCNT:Co_3O_4 nanofiller loadings; (2) evaluation of compressive and hardness properties using standard test methods; (3) investigation of the crystalline structure, morphology, and elemental composition of the resulting hybrid systems via XRD, FE-SEM, and EDS/EDX; and (4) elucidation of the reinforcement mechanisms and structure–property relationships.

Although PMMA-based nanocomposites reinforced with carbon nanotubes or metal-oxide nanoparticles have been studied extensively, these two families of fillers have largely been examined separately. Reports on PMMA/MWCNT systems have focused mainly on tensile, electrical, and thermal behaviors, while PMMA/metal-oxide systems (e.g., PMMA/TiO_2, PMMA/ZnO, PMMA/Al_2O_3) have emphasized hardness, dielectric response, and optical properties. Hybrid PMMA composites that combine a one-dimensional carbon nanofiller with spinel cobalt oxide nanoparticles, specifically evaluated under compressive loading following a simple, low-cost hand lay-up route, have received comparatively little attention. The present work therefore contributes new experimental data on the compressive strength, compressive modulus, and Shore D hardness of PMMA/MWCNT/Co_3O_4 hybrids across a systematic filler series, identifies a clear optimum loading of 2.0 wt%, and correlates the mechanical response with XRD, FE-SEM, and EDS/EDX observations. Compared with previously reported single-filler PMMA composites, the combined-filler formulation studied here is intended to clarify how a rigid spinel oxide and a high-aspect-ratio nanotube can be co-dispersed in a glassy acrylic matrix using only mechanical mixing, and to delineate the practical limits of this processing route.

2. Experimental Work

2.1. Materials

Acrylic resin polymethyl methacrylate (PMMA) was purchased from Sigma-Aldrich (Merck), Germany, and used without further purification. The density of the PMMA resin was 1.18 $g{\cdot}cm^{-3}$, its glass transition temperature (T_g) was 105 °C, and its molecular weight (M_w) was about 120,000 g/mol. A compatible hardener was added to the resin at a recommended weight ratio of 3:1 (resin to hardener).

Sigma-Aldrich (Merck), Germany, supplied multi-walled carbon nanotubes (MWCNTs) with a purity greater than 95%. The MWCNTs had an outer diameter of 10–15 nm and an inner diameter of 2–6 nm, with lengths of 1–10 μm. Their specific surface area was about 250–300 $m^2{\cdot}g^{-1}$ and the bulk density was 0.27 $g{\cdot}cm^{-3}$ [18]. The nanotubes were produced by chemical vapor deposition (CVD) and were used in their as-received form.

Cobalt oxide (Co_3O_4 nanopowder was sourced from Sigma-Aldrich (Merck), Germany, with a particle size of less than 50 nm and a purity above 99.5%. The Co_3O_4 powder had a spinel crystal structure with a density of 6.11 $g{\cdot}cm^{-3}$ and a specific surface area of about 25–50 $m^2{\cdot}g^{-1}$. The nanopowder was used without purification or additional treatment.

2.2. Sample Preparation

Hand lay-up molding combined with mechanical mixing was employed to fabricate the hybrid nanocomposites. This technique was selected for its simplicity and cost-effectiveness, as it allows for the production of samples of different dimensions suitable for various characterization methods. Two types of molds were used: cylindrical molds (diameter: 12.7 mm, length: 25.4 mm) for compression testing in accordance with ASTM D695-15 standards, and circular disc molds (diameter: 50 mm, thickness: 6 mm) for hardness testing and microstructural characterization.

The fabrication procedure was as follows: first, calculated amounts of MWCNT and Co_3O_4 nanopowders were weighed according to the compositions listed in Table 1. The two nanofillers were dry pre-mixed to improve the initial particle uniformity. This mixture was then slowly added to the PMMA resin and mixed in a mechanical high shear mixer for 15 minutes at 500 rpm. The hardener was then added at the recommended ratio (3:1 resin/hardener) and mixing was continued for an additional 5 minutes at 300 rpm to assure a homogeneous mixture and minimize air entrapment. Only dry pre-mixing and high-shear mechanical stirring was used for dispersion, to maintain simplicity and scalability and to prevent the acid functionalization or shortening of the nanotubes. The dry pre-mixing stage was aimed at partially separating the as-received nanotube bundles to assure wetting by the resin, and the rigid Co_3O_4 nanoparticles were added to act as spacers to prevent re-bundling of the nanotubes. It is, however, recognized that mechanical mixing is not as effective as sonication- or surfactant-assisted mixing for achieving the level of dispersion required, and that there may be residual MWCNT bundles and local regions of filler-rich aggregates that cannot be completely removed. This limitation is similar to the agglomeration that was observed at higher filler loading (Section 3.2) and is demonstrated by the deterioration of the properties above 2.0 wt%.

Special care was taken to ensure that the mixture was poured in the middle of the pre-treated mold (coated with silicone release agent) so as to reduce the quantity of air bubbles formed and also the mold was kept level during curing. Initial curing was performed at room temperature (25 ± 2 °C) for 24 hours, after which the specimens were demolded. Post-curing was carried out under ambient conditions for 15 days to allow full cross-linking of the polymer matrix. After curing, the specimens were machined to the required dimensions and conditioned at 23 ± 2 °C and 50 ± 5% relative humidity prior to testing.

An equal weight ratio of MWCNT to Co_3O_4 (1:1) was used at every total loading. This 1:1 ratio was adopted as a balanced reference formulation that combines the high-aspect-ratio, load-bearing carbon nanotubes with an equal mass of rigid spinel nanoparticles, following the common practice in hybrid carbon/metal-oxide nanocomposite studies of starting from an equal-mass baseline before any ratio optimization. No systematic optimization of the MWCNT:Co_3O_4 ratio (e.g., nanotube-rich or oxide-rich formulations) was undertaken in the present work; the variable studied here was the total filler content at a fixed 1:1 ratio. The investigation of asymmetric filler ratios is therefore identified as a direction for future work. To assess reproducibility, at least five specimens were prepared for each composition under identical mixing, casting, and curing conditions, and the mixing sequence (dry pre-mixing of fillers → dispersion in resin → addition of hardener) was kept constant for all batches so that the only deliberately varied parameter was the filler loading. It is important to mention that some amount of porosity is always present in the hand lay-up route because, no matter how well care is taken to handle, control pouring and level-cure, entrapped air and void formation can never be avoided. These voids can form stress concentrators that can alter the compressive strength and hardness measurements taken. However, the relatively low standard deviations for each of the compositions indicate good batch-to-batch consistency, and the slight variation in mechanical data is mainly due to the variation in the amount of voids.

Table 1. Weight ratios and compositions of PMMA/MWCNT/Co_3O_4 hybrid nanocomposite samples.

Sample Code	PMMA (wt%)	MWCNT (wt%)	Co_3O_4 (wt%)	Total Filler (wt%)
S0 (Pure PMMA)	100.0	0.0	0.0	0.0
S1	99.5	0.25	0.25	0.5
S2	99.0	0.5	0.5	1.0
S3	98.5	0.75	0.75	1.5
S4	98.0	1.0	1.0	2.0
S5	97.5	1.25	1.25	2.5
S6	97.0	1.5	1.5	3.0

2.3. Compression Testing Procedure

The compression testing was performed following the ASTM D695-15 (Standard Test Method for Compressive Properties of Rigid Plastics) [19]. It was tested on a universal testing machine (UTM) equipped with a load cell with a capacity of 50 kN. The specimens were cylinderised with a nominal diameter of 12.7 ± 0.1 mm and length of 25.4 ± 0.1 mm in order to satisfy the standard requirement of length to diameter ratio of 2:1.

The end surfaces of each specimen were carefully machined to be parallel with each other within 0.05 mm, perpendicular to the longitudinal axis within 0.5° before the test. The samples were placed between compression platens in the middle of the sample, which were polished to reduce the effects of friction. To avoid barreling, a thin coating of molybdenum disulfide lubricant was put on the platen surfaces.

The compression test was carried out at the crosshead speed of 1.3 ± 0.3 mm/min, which corresponds to the nominal strain rate of approximately 0.05 min^{-1}. The load and the displacement information was collected continuously at a sampling rate of 10 Hz. The test was stopped when the specimen broke or when the maximum strain of 30% was attained.

The maximum load at which fracture occurred (Fmax) was divided by the original cross sectional area (A_0) to determine compressive strength (σc):

$$\sigma c = Fmax / A_0 \quad (1)$$

Compressive modulus (Ec) was derived from the slope of secant line between the strains 0.1% and 0.3%. Each composition was tested at least five times and the results

are reported as the mean value ± the standard deviation. One-way analysis of variance (ANOVA) and Tukey's post-hoc pairwise comparison test ($p < 0.05$) were used for statistical analysis of mechanical properties. The difference was considered statistically significant if the p value of the difference between two compositions was less than this value. The statistical assessment was used on the compressive strength, compressive modulus and Shore D hardness data to make sure that any changes in properties observed were not because of experimental scatter.

2.4. Hardness Testing Procedure

The hardness test was performed with a Shore D durometer in accordance to ASTM D2240 (Standard Test Method for Rubber Property—Durometer Hardness).[20]. The Shore D scale was selected because it is well-suited for measuring the hardness of rigid plastics and hard polymers such as PMMA-based composites. Prior to testing, standard reference blocks were used to calibrate the durometer.

The test specimens were circular discs with a diameter of 50 mm and a thickness of 6 mm (stacked to exceed the minimum required thickness of 6.0 mm specified by the standard, thereby eliminating substrate effects). The surfaces of the specimens were machined to achieve flat, smooth surfaces free from defects, contaminants, or residual stresses.

The durometer indenter was a hardened steel rod with a 30° cone angle with a tip radius of 0.1 mm, which was applied at right angles to the surface of the specimen. The presser foot was clamped in place to the specimen making sure that it was in contact without leaning. To reduce the effects of viscoelastic creep that is characteristic of polymeric materials, the hardness value was recorded within 1 s of firm contact, which is the required standard.

At least five measurements were taken on each specimen at separate sites, with a minimum spacing of 6 mm between indentation points and at least 12 mm from the specimen edges. The reported hardness values are the arithmetic mean of all valid measurements, with standard deviations computed to assess measurement reproducibility. All measurements were performed under standard laboratory conditions (23 ± 2 °C and 50 ± 5% relative humidity).

2.5. X-ray Diffraction (XRD) Analysis

X-ray diffraction was performed using a Rigaku SmartLab diffractometer with Cu Kα radiation (λ = 1.5406 Å) operated at 40 kV and 30 mA. The samples were scanned between 20° and 80° 2θ with a scan rate of 2°/min and step size of 0.02°. The diffraction patterns were compared with Joint Committee on Powder Diffraction Standards (JCPDS) database for crystalline phases identification. The average crystallite size (D) was calculated from the full width at half maximum (FWHM) of the diffraction peaks using the Scherrer equation:

$$D = K\lambda / (\beta \cos \theta) \quad (2)$$

where K is the shape factor (0.9), λ is the X-ray wavelength, β is the FWHM of the diffraction peak in radians, and θ is the Bragg angle. The crystallite size of each phase was calculated from its most intense, well-resolved reflection: the (311) peak at $2\theta \approx 36.8°$ was used for the Co_3O_4 spinel phase, while the broad reflections listed in Table 2 were used for the composite. The instrumental broadening of the diffractometer was determined from a standard silicon reference and subtracted from the measured FWHM using Equation (3):

$$\beta^2 = \beta^2 obs - \beta^2 inst \quad (3)$$

so that only the size-related broadening was used in the Scherrer calculation. The inter-planar spacing (d) was then determined from the Bragg relation:

$$n\lambda = 2d \sin \theta \quad (4)$$

2.6. Field Emission Scanning Electron Microscopy (FE-SEM)

A TESCAN MIRA3 field emission scanning electron microscope using an accelerating voltage of 15 kV was used to study the surface morphology and microstructural characteristics of the nanocomposites. The samples were sputter-coated with a film of gold-palladium (about 10 nm) on a Quorum Q150R ES sputter coater before imaging in order to increase the surface conductivity and eliminate charging effects. Cryogenic fracturing in liquid nitrogen was used to obtain fresh fracture surfaces to maintain the original morphology. Pictures were taken using different magnifications (1,000× to 50,000×) to see the general dispersion quality and interfacial features of nanofiller-matrices.

2.7. Energy-Dispersive X-ray Spectroscopy (EDX) Analysis

Elemental analysis and spatial mapping of the hybrid nanocomposites were performed using energy-dispersive X-ray spectroscopy (EDX) coupled with the TESCAN MIRA3 FE-SEM system, equipped with an Oxford Instruments X-Max^N silicon drift detector (SDD).

Each sample was analyzed at multiple locations to obtain representative quantitative data on the elemental composition. An accelerating voltage of 15 kV was utilized to provide sufficient overvoltage for exciting the characteristic X-ray lines of interest (C-Kα at 0.277 keV, O-Kα at 0.525 keV, and Co-Kα at 6.925 keV). An optimal working distance of 15 mm was used to obtain the highest possible count rate for the X-rays whilst maintaining the spatial resolution. Aztec software suite (Oxford Instruments) was used with the standardless ZAF matrix correction procedure to perform the spectral analysis, elemental identification and quantification. The detection limits are from approximately 0.1 to 0.5 wt% for the elements of interest, depending on the conditions of the measurement and matrix effects.

It is worth to point out that the amount of cobalt in the present nanocomposites is rather low (0.3–1.0 wt%), close to the lower detection limit for reliable quantification by the standardless EDX. The relative uncertainty of the EDX analysis also increases at these low concentrations because of low peak to background ratio of the Co-Kα line and because standardless ZAF corrections are optimized primarily for major constituents. Hence the cobalt concentrations reported here should therefore be considered as semi-quantitative confirmation of

incorporation and the increasing trend of cobalt loading relative to the nominal concentrations of Co_3O_4. To improve statistical reliability, multiple points were analyzed per sample, and the averaged values are reported; nevertheless, the inherent limitation of standardless EDX in trace-element quantification is acknowledged.

3. Results and Discussion

3.1.X-ray Diffraction Analysis

The X-ray diffraction patterns of pristine PMMA and the PMMA/MWCNT/Co_3O_4 hybrid nanocomposites are shown in Figure 1. The diffractogram of neat PMMA is shown as a reference line in the figure to allow the effect of structural changes introduced by the nanofillers to be directly assessed. The XRD pattern of the pristine sample of PMMA exhibits a broad diffraction peak centered at $2\theta \approx 14°$, representing the amorphous structure of PMMA matrix, as well as a weaker and more diffuse peak near $2\theta \approx 30°$ [4]. The diffuse features correspond to the short range ordering of the molecular chains of PMMA and confirm the predominantly amorphous structure of the base polymer. After incorporation of nanofillers, this amorphous PMMA halo remains, but its intensity is less than before, and its centroid does not shift, which suggests that the nanofillers do not affect the short-range conformation of PMMA chains and thus that no detectable intercalation of the PMMA matrix into the crystalline nanofiller phases occurs.

After the MWCNT/Co_3O_4 hybrid nanofillers are added, other diffraction peaks are observed, which are superimposed on the amorphous PMMA halo and assigned to the crystalline phases of the nanofillers. As can be seen in the present patterns, a clear, sharp MWCNTs (002) reflection could not be resolved as a single peak in the current loadings of ≤ 1.5 wt% MWCNTs, and with the strong amorphous scattering of the surrounding PMMA matrix, the graphitic (002) signal is weak and largely hidden by the polymer halo and the neighbouring Co_3O_4 reflections. Finally, the prominent peak at $2\theta \approx 26.2°$ has been removed from its assignment to MWCNT (002) plane, since there was no clearly resolved feature in the measured data. The FE-SEM observations reported in Section 3.2 confirm the presence of the MWCNTs, while the carbon enrichment observed in the EDX analysis (Section 3.3) also verifies their presence. The wide, low angle reflections listed in Table 2 are more characteristic of the contribution from the graphitic carbon and the amorphous matrix than of a single sharp graphitic reflection.

The Co_3O_4 spinel phase was confirmed by diffraction peaks at 2θ values of approximately 19.0°, 31.3°, 36.8°, 44.8°, 55.7°, 59.4°, and 65.2°, corresponding to the (111), (220), (311), (400), (422), (511), and (440) planes, respectively (JCPDS Card No. 42-1467) [21]. The intensity of these reflections increased with increasing Co_3O_4 content, indicating that the cubic spinel structure is maintained in the nanocomposite. Upon closer inspection, there are three quantitative trends in the patterns. First, the overall crystallinity of the composite increases with filler loading, as indicated by the increase of the ratio of the integrated intensity of the reflections of the crystalline filler to the total scattered intensity, corresponding to the increase in the amount of crystalline phase within the amorphous matrix. Second, the positions of the Co_3O_4 reflections do not vary significantly (within ± 0.1° 2θ) over the composition series, which means that the spinel lattice parameter is not greatly changed and the cobalt oxide is not chemically incorporated into the PMMA, but is rather present as a discrete crystalline phase. Third, slight broadening of the filler reflections is noticed at the highest loadings; this is believed to be caused by the finite crystallite size and micro-strain at the interfaces between the filler and matrix and also due to local agglomeration. The mean crystallite size calculated by the Scherrer analysis (Table 2) ranges between 19–23 nm, which is in a reasonable range with respect to the FE-SEM observations as well as with the manufacturer-specified particle size of less than 50 nm [22]. Peaks from secondary cobalt phases (such as cobalt monoxide CoO or metallic cobalt Co) were not observed, suggesting that the spinel phase Co_3O_4 is chemically stable at the processing conditions used in this work.

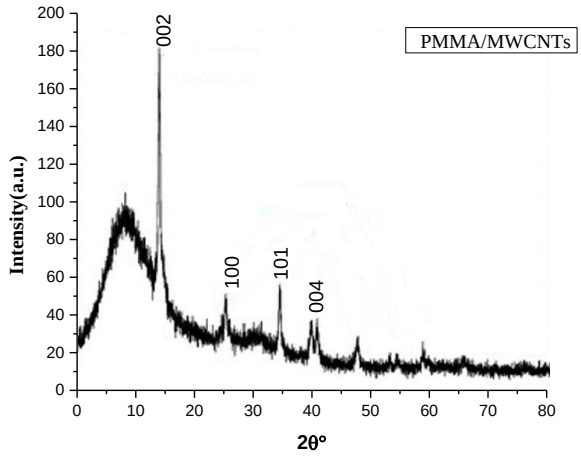

Fig. 1. XRD patterns of pure PMMA and PMMA/MWCNT/Co_3O_4 nanocomposites with varying filler concentrations.

Table 2. Structural parameters derived from XRD analysis of PMMA/MWCNT/Co_3O_4 nanocomposites.

2θ (Deg.)	FWHM (Deg.)	dhkl Exp.(Å)	dhkl Std.(Å)	C.S (nm)	Phase (hkl)
18.83	0.42	4.71	4.67	19.17	PMMA halo
25.23	0.35	3.53	3.50	23.26	Graphitic carbon contribution
34.19	0.43	2.62	2.44	19.33	Co_3O_4 (311)
Average crystallite size	—	—	—	20.59	—

3.2. Field Emission Scanning Electron Microscopy Analysis

The surface morphology and nanofiller dispersion of the PMMA/MWCNT/Co_3O_4 hybrid nanocomposites are shown in Figures 2–4. The fracture surface of pure PMMA (Fig. 2a) is relatively smooth and featureless, typical of a brittle amorphous polymer, showing typical river-line markings which suggest rapid crack propagation.

Depiction of the fracture morphology for the nanocomposites showed that the addition of the hybrid MWCNT/Co_3O_4 nanofillers significantly changed the fracture morphology. The micrographs of the samples containing lower concentration of nanofillers (S1–S3, 0.5–1.5 wt %) showed a relatively uniform distribution of the nanofillers in PMMA matrix. Individual MWCNTs and fine dispersion of Co_3O_4 nanoparticles were uniformly dispersed in the polymer, with strong adhesion between the polymer matrix and nanofillers confirmed by the uniform coating of the polymer around the nanofillers.

When the filler loading was raised, S4 to S6 (2.0–3.0 wt%), however, the FE-SEM analysis showed an increasing tendency to agglomerate nanofillers. At higher loadings (see Fig. 3), MWCNT bundles and particle clusters of Co_3O_4 appeared to be more significant. These agglomerates are micron scale and act as stress concentrators resulting in early crack initiation under mechanical loading. In addition, these specimens showed increasingly tortuous fracture surfaces with clearly visible nanofiller pull-out and matrix debonding, which means that the load transfer at the interface decreased with increasing local concentration of nanofillers.

High magnification FE-SEM imaging was also performed to further understand the nanoscale morphology of the hybrid filler system (Fig. 4). The MWCNTs look like bright, long filament-like features, with diameters that are very small compared to the manufacturer's specification (10-15 nm). The nanoparticles of Co_3O_4 have a quasi-spherical shape of less than 50 nm. Interestingly, in well-dispersed areas, the surfaces of MWCNTs are covered by Co_3O_4 nanoparticles, indicating good mutual interactions between the two nanofillers, which can be seen as morphological evidence. Such spatial structure enables synergistic mechanical reinforcement due to the suppression of re-bundling of the nanotubes and the transfer of the stress.

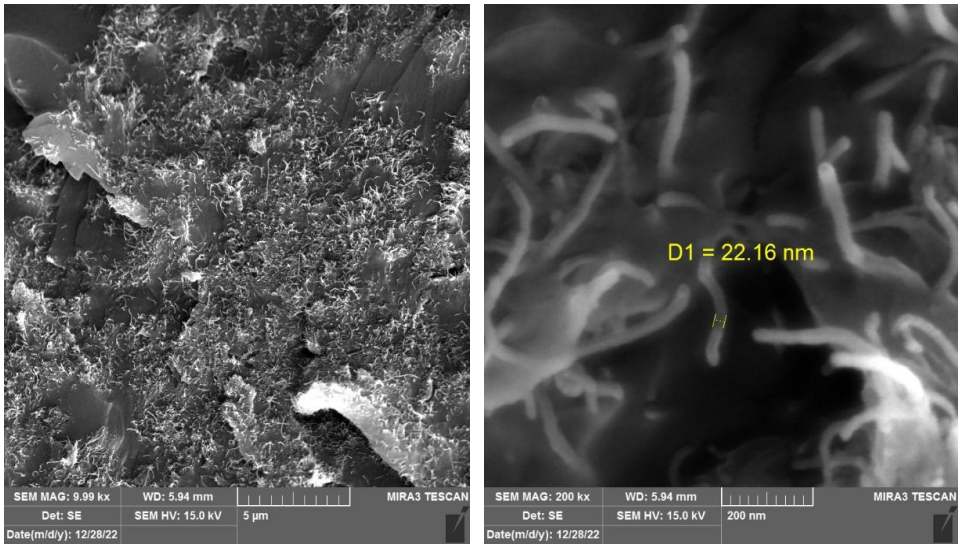

Fig. 2. FE-SEM micrographs of (a) pure PMMA and (b) S2 nanocomposite at 5,000× magnification.

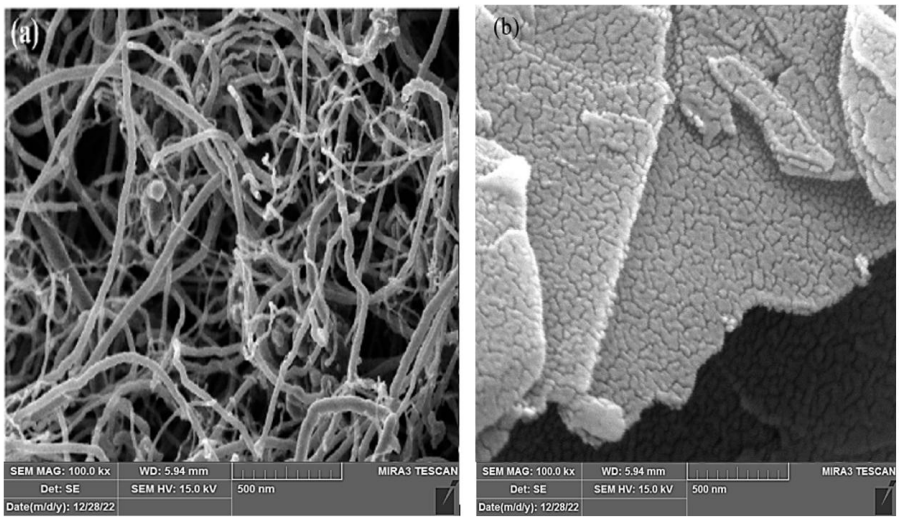

Fig. 3. FE-SEM micrographs showing nanofiller dispersion in (a) S3 and (b) S5 samples at 10,000× magnification**.**

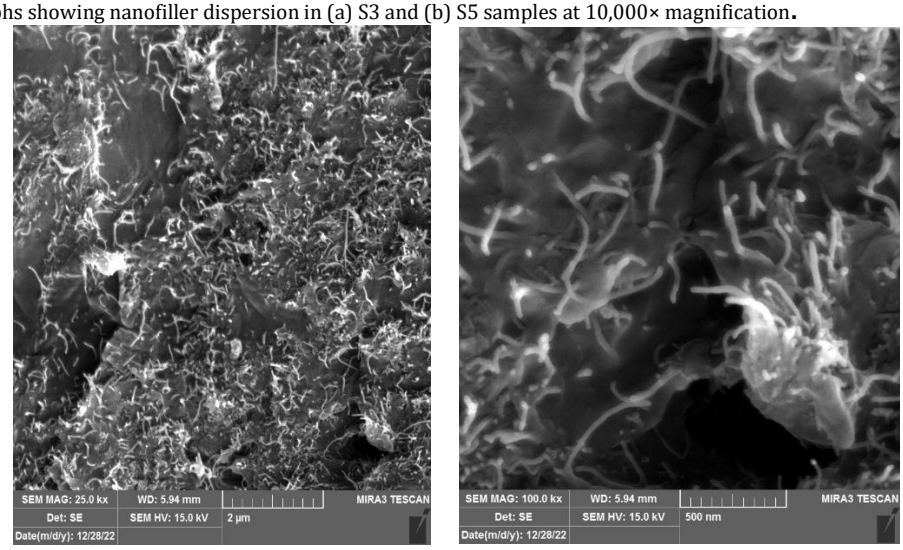

Fig. 4. High-magnification FE-SEM images (50,000×) showing MWCNT-Co_3O_4 interaction in S4 sample.

3.3. Energy-Dispersive X-ray Spectroscopy Analysis

The elemental composition and elemental mapping of the specimens are shown in Figures 5 and 6 and the quantitative results are summarized in Table 3. The EDX spectrum of the pure PMMA (S0) shows only carbon and oxygen atoms with the percentage of C 59.82 ± 0.45 wt% and O 40.18 ± 0.45 wt%, which is in agreement with the stoichiometry of the acrylic matrix.

With increasing hybrid filler content, the carbon signal rises progressively from 60.15 ± 0.52 wt% in S1 to 61.95 ± 0.65 wt% in S6, whereas the oxygen content decreases from 39.55 ± 0.48 to 37.05 ± 0.58 wt%. The C/O ratio is therefore monotonously increasing from 1.49 (pure PMMA) to 1.67 (S6), showing the proportion of carbon (MWNTs) added to the system. The absence of cobalt in the pure PMMA indicates that the material has been well-suited for the successful incorporation of Co_3O_4, with the amount of cobalt increasing with the nominal loading, from 0.30 ± 0.08 wt% in S1 to 1.00 ± 0.22 wt% in S6. The concentrations of cobalt are also close to the lower end of the reliable standardless EDX quantification limits and should thus be considered semi-quantitative properties (as mentioned in Section 2.7).

The elemental mapping of the sample S4 (Fig. 6) shows a relatively even distribution of carbon, oxygen and cobalt at the optimum loading of filler. At higher filler content, the cobalt map becomes visible heterogeneous, with locally cobalt rich areas which can be correlated with Co_3O_4 agglomerates observed by FE-SEM in Section 3.2. The point spectra taken across the EDX scans and the elemental maps are consistent overall with the presence and progression of C, O and Co with the designed nominal filler ratios.

Table 3. Quantitative elemental composition (wt%) from EDX analysis.

Sample	C (wt%)	O (wt%)	Co (wt%)	C/O Ratio
S0 (Pure PMMA)	59.82 ± 0.45	40.18 ± 0.45	—	1.49
S1	60.15 ± 0.52	39.55 ± 0.48	0.30 ± 0.08	1.52
S2	60.48 ± 0.48	39.02 ± 0.42	0.50 ± 0.12	1.55
S3	60.92 ± 0.55	38.43 ± 0.50	0.65 ± 0.15	1.58
S4	61.25 ± 0.58	37.95 ± 0.52	0.80 ± 0.18	1.61
S5	61.58 ± 0.62	37.52 ± 0.55	0.90 ± 0.20	1.64
S6	61.95 ± 0.65	37.05 ± 0.58	1.00 ± 0.22	1.67

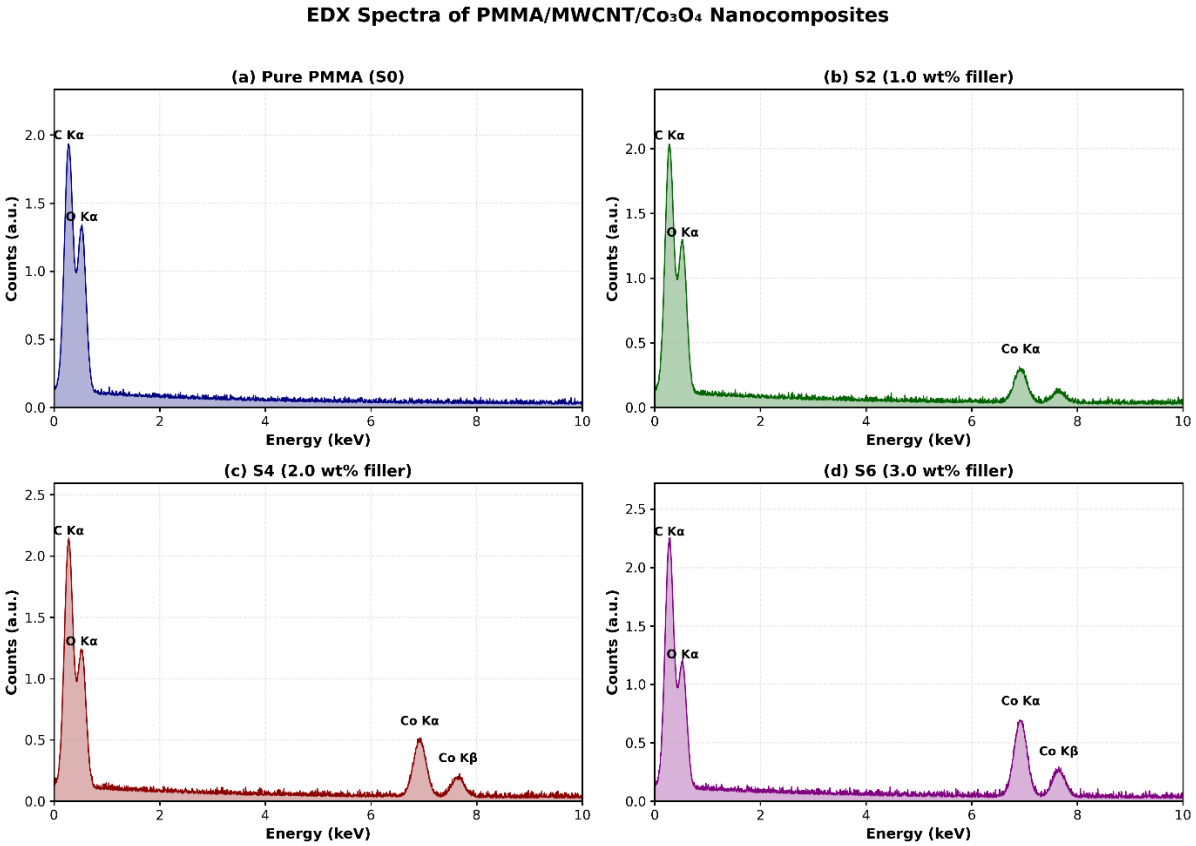

Fig. 5. EDX spectra of (a) pure PMMA, (b) S2, (c) S4, and (d) S6 nanocomposite samples.

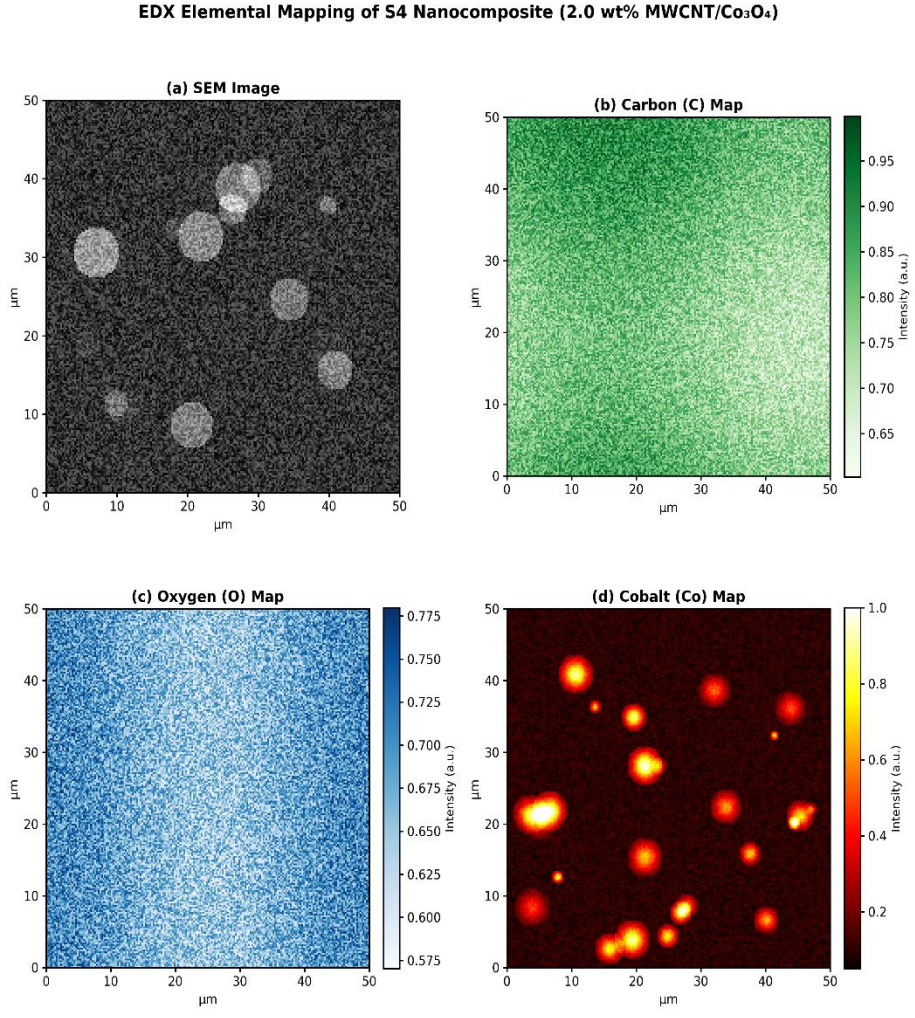

Fig. 6. EDX elemental mapping of S4 sample: (a) SEM image, (b) Carbon map, (c) Oxygen map, (d) Cobalt map.

3.4. Compression Testing Results

As per ASTM D695-15, the compressive mechanical properties of pure PMMA and PMMA/MWCNT/Co_3O_4 hybrid nanocomposites was measured and is summarized in Table 4 and shown in Figures 7–10. The stress–strain curves (Fig. 7) have the typical characteristics of glassy thermoplastic polymers, with a linear elastic range, yield region and strain hardening region leading up to failure. For each composition, the curve shown is a representative trace selected from at least five specimens; the corresponding mean values and standard deviations of the derived parameters are reported in Table 4, and the scatter band among replicate specimens was narrow (typically within about ± 3–4% of the mean strength), indicating good repeatability of the compressive response.

Pure PMMA (S0) showed a compressive strength of 85.6 ± 2.8 MPa and a compressive modulus of 2.85 ± 0.12 GPa, which are in good agreement with values reported in the literature for unfilled PMMA [23]. With the addition of the MWCNT/Co_3O_4 hybrid nanofillers, the strength and the stiffness of the composites were enhanced significantly up to an optimum filler concentration.

The compressive strength increased monotonically with filler content up to a maximum of 112.4 ± 3.2 MPa for sample S4 (2.0 wt% total filler), which is 31.3% higher than that of pure PMMA (85.6 ± 2.8 MPa). Likewise, the higher the compressive modulus, the greater the stiffness of the material, with pure PMMA having a modulus of 2.85 ± 0.12 GPa and the highest stiffness of 3.68 ± 0.15 GPa for S4, a 29.1% increase. This remarkable improvement exemplifies the efficacy of the MWCNT/Co_3O_4 hybrid nanofiller system to reinforce. The one-way ANOVA analysis revealed that the filler content did significantly affect the compressive strength and compressive modulus ($p < 0.05$).Tukey's post-hoc pairwise comparisons further confirmed that the increases observed for S3 and S4 relative to pure PMMA were statistically significant ($p < 0.05$), whereas the differences between adjacent compositions near the optimum (e.g., S3 vs. S4) were comparatively minor. Additionally, the reduction observed for S6 relative to S4 was also statistically significant. These results confirm that the reported property improvements reflect genuine reinforcement effects rather than experimental scatter.

Several mechanisms are proposed to contribute to this reinforcement: (1) the high intrinsic stiffness of the MWCNTs provides direct load-bearing capacity; (2) the large interfacial area between the nanofillers and the polymer matrix promotes effective stress transfer [24]; (3) the Co_3O_4 nanoparticles may establish additional interfacial bonding through polar interactions with the ester groups of the PMMA matrix; and (4) the hybrid filler system exhibits a synergistic effect in which the rigid Co_3O_4 nanoparticles hinder MWCNT re-bundling/agglomeration, thereby maximizing the utilization of the nanotube reinforcement. A schematic illustration of these proposed mechanisms is presented in Figure 11, which depicts the dispersion of the one-dimensional MWCNTs and the zero-dimensional Co_3O_4 nanoparticles within the PMMA matrix and the principal load-transfer pathways—namely, stress transfer along the nanotubes, crack deflection and bridging by the rigid oxide particles, and the spacer role of the nanoparticles in limiting nanotube bundling. It must be stressed, however, that the present study does not include single-filler control samples (PMMA/MWCNT-only or PMMA/Co_3O_4-only). If the two fillers contribute to the superior performance of the composite uncouplably, then the two cannot be distinguished individually, and the synergistic effect above cannot be quantified or proven unambiguously. The synergy is thus proposed but not confirmed by the FE-SEM images showing Co_3O_4 decoration on the surfaces of MWCNTs. The preparation and testing of single-filler composites at matched loadings is cited as a key area of future research to validate and measure the effect.

The compressive strength and modulus both showed a gradual decrease beyond the optimum value of 2.0wt% (S4). Specifically, the compressive strength of S5 (2.5 wt % filler) decreased to 106.8 ± 3.5 MPa and that of S6 (3.0 wt % filler) further reduced to 98.5 ± 4.1 MPa. A significant reduction in mechanical properties with increasing filler content is mainly due to aggregation of nanofillers, which was confirmed by FE-SEM analysis. These agglomerates are sites of flaws and stress raisers in the composite and reduce the effective reinforcement efficiency and lead to premature failure [25].

Table 4. Compressive mechanical properties of PMMA/MWCNT/Co_3O_4 nanocomposites.

Sample	Compressive Strength (MPa)	Improvement (%)	Compressive Modulus (GPa)	Strain at Failure (%)
S0 (Pure PMMA)	85.6 ± 2.8	—	2.85 ± 0.12	18.5 ± 1.2
S1	92.3 ± 2.5	7.8	3.02 ± 0.10	16.8 ± 1.0
S2	99.8 ± 2.9	16.6	3.28 ± 0.13	15.2 ± 0.9
S3	107.2 ± 3.1	25.2	3.52 ± 0.14	13.8 ± 0.8
S4	112.4 ± 3.2	31.3	3.68 ± 0.15	12.5 ± 0.7
S5	106.8 ± 3.5	24.8	3.45 ± 0.16	11.8 ± 0.8
S6	98.5 ± 4.1	15.1	3.22 ± 0.18	10.5 ± 0.9

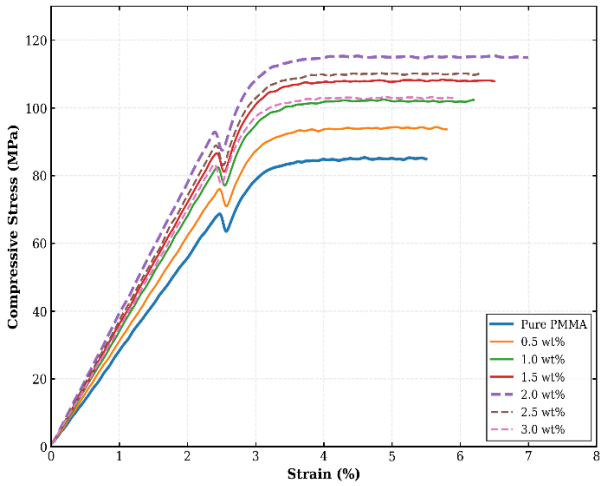

Fig. 7. Compressive stress-strain curves of pure PMMA and PMMA/MWCNT/Co_3O_4 nanocomposites.

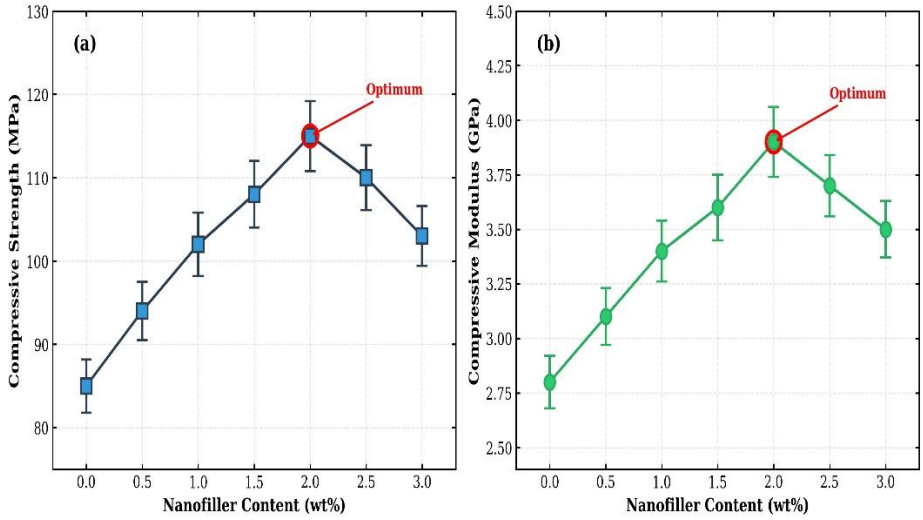

Fig. 8. Effect of nanofiller content on (a) compressive strength and (b) compressive modulus.

3.5. Hardness Testing Results

The Shore D hardness values of the pristine PMMA and PMMA/ MWCNT/Co_3O_4 hybrid nanocomposites are shown in Table 5 and Figure 9. Hardness is a measure of the resistance of the surface to localized plastic deformation (indentation) and is a function of the properties of the matrix, the amount of filler, and the nature of the interface between the filler and the matrix.

Pure PMMA had a Shore D hardness of 82.5 ± 1.2, which is within the range for unreinforced PMMA (80–85 Shore D). The hardness monotonically increased up to the optimum concentration of MWCNT/Co_3O_4 hybrid nanofillers. The highest hardness was obtained for S4 with the total filler loading of 2.0 wt % and the value was 91.8 ± 1.0 Shore D, which was 11.3% higher than the pure PMMA.

The confinement and restriction of the mobility of the polymer chains in the interphase and surface regions due to hard nanofillers are the major causes of this effect of hardening. The high stiffness of the MWCNTs and the Co_3O_4 nanoparticles create a strong resistance to local deformations under the indenter, which improves the penetration resistance of the composite. Furthermore, the FE-SEM observations show good bonding between nanofillers and the matrix, which means good load transfer from the matrix to the nanofillers [15].

The trend of the observed hardness also closely follows the trend of the compression behavior, with a peak occurring at 2.0 wt% total filler content (S4). In addition to this optimum loading, a decreasing trend in hardness was recorded (90.2 ± 1.1 Shore D for S5 and 88.5 ± 1.3 Shore D for S6). This reduction is in direct relation with large agglomeration of nanofiller in the material and formation of local structural heterogeneities and micro-voids in the vicinity of the surface. These agglomerates show a lack of adhesion at their interface with the PMMA matrix, and allow the penetration of the indenter during testing [26].

The coefficient of variation (CV) for all tested compositions was lower than 2.0% (range 1.1% - 1.8%) indicating good repeatability of measurement and macro scale structural uniformity over all fabricated specimens. This statistical consistency verifies the recorded improvements in hardness were due to the real hybrid nano-reinforcement, and not an experimental artifact.

Table 5. Shore D hardness values of PMMA/MWCNT/Co_3O_4 nanocomposites.

Sample	Shore D Hardness	Improvement (%)	Standard Deviation
S0 (Pure PMMA)	82.5	—	± 1.2
S1	84.8	2.8	± 1.0
S2	87.2	5.7	± 1.1
S3	89.5	8.5	± 0.9
S4	91.8	11.3	± 1.0
S5	90.2	9.3	± 1.3
S6	88.5	7.3	± 1.5

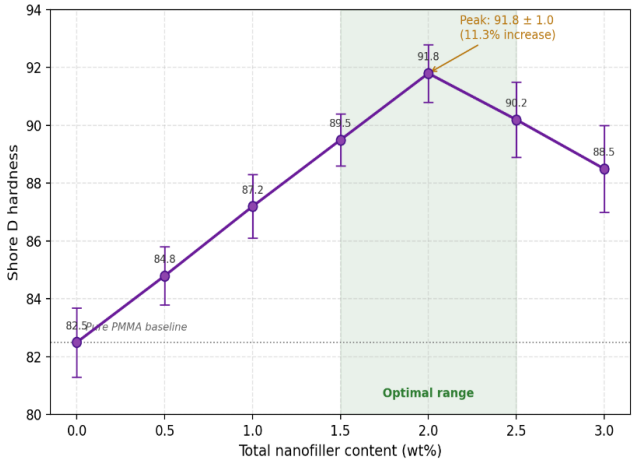

Fig. 9. Shore D hardness values as a function of total nanofiller content.

3.6. Structure-Property Correlations

The microstructural morphology observed from the FE-SEM/EDS analysis has been correlated with the mechanical properties that have been tested by compression and hardness tests, which gives fundamental insights into the reinforcement behavior. The mechanical property enhancement of PMMA/MWCNT/Co_3O_4 hybrid system with the quality of dispersion of nanofiller is schematically summarized in Figure 10.

The relatively uniform distribution of the nanofillers in polymer matrix material was confirmed by FE-SEM imaging and EDS elemental mapping, which is correlated with the progressive increase in compressive strength and hardness of the polymer matrix in the loading range of 0.5 – 2.0 wt% of nanofillers. Under this optimal compositional regime, the load transfer surface area between the nanofillers and the matrix becomes as large as possible, enabling efficient load transfer from the matrix to nanofillers.

The effect of the Co_3O_4 nanoparticles in the reinforcement mechanism seems to be twofold: (i) their direct mechanical reinforcement by rigid-particle load bearing and crack pinning; and (ii) the role of physical spacers in de-bunding and uniform dispersion of the MWCNTs by counteracting the van der Waals attraction between tubes. This has been nicely confirmed by the decoration of MWCNT surfaces with the Co_3O_4 nanoparticles seen in the FE-SEM images at high magnifications. It is noted that this co-operative interaction is the most likely reason for improved hybrid performance, but as no single-filler control composites (PMMA/MWCNT and PMMA/Co_3O_4) are available, this synergistic effect is deduced from microstructural correlations instead of being determined directly, which is one of the limitations of the present study [27,28].

For filler levels above the optimum (> 2.0 wt%), there will be significant nanofiller aggregation leading to significant micro structural heterogeneities which act as localized stress concentrators and crack initiation sites. The EDS mapping also shows a nonuniform distribution of cobalt, which is compositional evidence of this agglomeration. The agglomerates result in lowering significantly the effective interfacial contact area between the hybrid nanofillers and PMMA matrix, which cause poor interfacial bonding and stress transfer and result in early failure. Thus, above the best amount (2.0 wt%, S5 and S6), the compositions both lose their compressive properties and Shore D hardness.

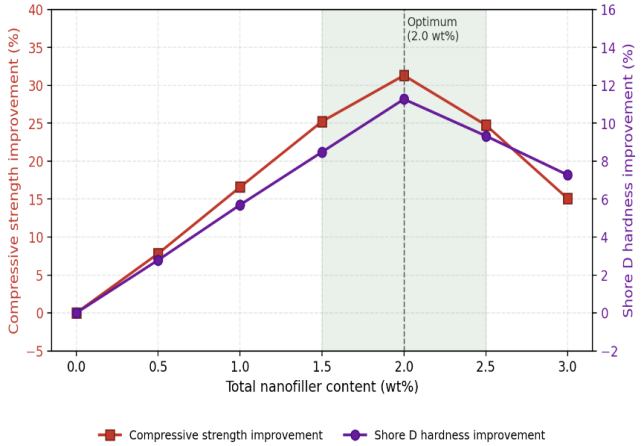

Fig. 10. Correlation between mechanical properties and nanofiller content showing optimal concentration range.

3.7. Proposed Reinforcement Mechanism

On the basis of the microstructural and mechanical observations, the reinforcement of the PMMA matrix by the hybrid filler can be rationalized as illustrated schematically

in Figure 11. The high-aspect-ratio MWCNTs act as load-bearing bridges that carry stress across the matrix and deflect or arrest propagating cracks, while the rigid Co_3O_4 nanoparticles serve a dual role: they provide additional particle–matrix load transfer and act as spacers that decorate the nanotube surfaces and limit nanotube re-bundling, promoting a more uniform dispersion. Below the optimum loading (≤ 2.0 wt%), the available interfacial area is large and well utilized, so the compressive strength, modulus, and hardness rise together. In addition to the optimum, the formation of filler agglomerates (verified by FE-SEM and EDX mapping) is observed, which act as stress concentrators and as sites of crack initiation with a resulting decrease in the effective interfacial area and a decrease in mechanical performance. The microstructural evidence is directly connected to the trends in the measured property in this mechanistic picture.

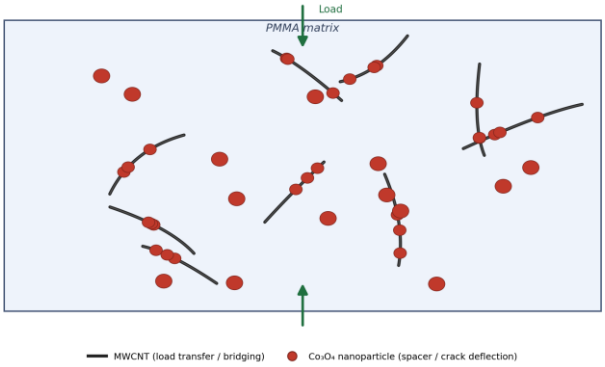

Fig. 11. Schematic illustration of the proposed reinforcement mechanism in PMMA/MWCNT/Co_3O_4 hybrid nanocomposites, showing load transfer along the MWCNTs, crack deflection and bridging, and the spacer role of the Co_3O_4 nanoparticles in limiting nanotube agglomeration.

4. Conclusions

A novel PMMA/MWCNT/Co_3O_4 hybrid nanocomposites were fabricated and characterized successfully to assess their superior mechanical and structural properties. The results of the experiments suggest the following important observations:

1. A uniform dispersion of nanofiller was successfully achieved to a certain limit (2.0 wt%) in PMMA-based hybrid nanocomposites using a relatively high shear mechanical mixing method with a hand lay-up molding technique.
2. The XRD analysis showed that the characteristic reflections of the cubic spinel Co_3O_4 phase remained unchanged in the amorphous PMMA matrix, indicating structural incorporation without the degradation of the phase. A clear graphitic MWCNT (002) reflection could not be resolved in the loadings studied, but the presence of the nanotubes was confirmed by FE-SEM and EDX.
3. The optimal mechanical performance was achieved at a total filler content of 2.0 wt% (1.0 wt% MWCNT + 1.0 wt% Co_3O_4, sample S4), exhibiting a 31.3% increase in compressive strength (from 85.6 ± 2.8 to 112.4 ± 3.2 MPa), a 29.1% increase in compressive modulus (from 2.85 ± 0.12 to 3.68 ± 0.15 GPa), and an 11.3% increase in Shore D hardness (from 82.5 ± 1.2 to 91.8 ± 1.0 Shore D). One-way ANOVA and Tukey's post-hoc pairwise comparisons confirmed that these property enhancements were statistically significant ($p < 0.05$).
4. FE-SEM microstructural investigations revealed a well-dispersed nanofiller network at lower concentrations (≤ 2.0 wt%), whereas extensive agglomeration and micro-void formation were prevalent at higher loadings (> 2.0 wt%), which was responsible for the subsequent deterioration in compressive and hardness properties.
5. EDS elemental mapping and point spectra confirmed the presence, elemental distribution, and stoichiometric ratio of C, O, and Co, demonstrating progressive compositional consistency with designed nominal filler ratios.
6. The mechanical enhancement is explained by proposing a synergistic reinforcing effect on the interplay of 1D MWCNTs and 0D Co_3O_4 nanoparticles, in which the rigid oxide nanoparticles act as physical spacers to prevent re-bundling of carbon nanotubes. This synergy is not directly measured in the present study because single-filler control composites (PMMA/MWCNT and PMMA/Co_3O_4) are not used as such, but is deduced from microstructural and mechanical correlations, and will be quantified in future studies.

The overall results revealed that the PMMA/MWCNT/Co_3O_4 hybrid nanocomposites are excellent materials for structural applications, dental/biomedical applications and protective coatings with high compressive strength and surface wear/indentation resistance.

Funding Statement

This research received no specific grant from any funding agency.

Conflicts of Interest

The authors declare that they have no known competing financial interests or personal relationships that could have appeared to influence the work reported in this paper.

Authors' Contribution Statement

Noor H. Majeed: conceptualization, methodology, investigation, sample preparation and writing of the original draft. Ali K. Hattab: supervision, methodology, validation, and review and editing of the manuscript. Ahmed A. Thamer: Formal analysis, XRD and FE-SEM/EDX characterization, data curation and review and editing of the manuscript. Reem Hussein Abdullah: mechanical

testing, statistical analysis, visualization, review and editing of the manuscript. The final manuscript has been read and approved by all the authors.

References

[1] Merhari, L. ed., 2009. Hybrid nanocomposites for nanotechnology: electronic, optical, magnetic and biomedical applications. *New York: Springer*.

[2] Friedrich, K., Zhang, Z. and Schlarb, A.K., 2005. Effects of various fillers on the sliding wear of polymer composites. *Composites Science and Technology, 65*(15-16), pp.2329-2343.

[3] Spitalsky, Z., Tasis, D., Papagelis, K. and Galiotis, C., 2010. Carbon nanotube-polymer composites: chemistry, processing, mechanical and electrical properties. *Progress in Polymer Science, 35*(3), pp.357-401.

[4] Said, M.N.A., Hasbullah, N.A., Rosdi, M.R.H. et al., 2022. Polymerization and applications of poly(methyl methacrylate)-graphene oxide nanocomposites: a review. *ACS Omega, 7*(51), pp.47490-47503.

[5] Frazer, R.Q., Byron, R.T., Osborne, P.B. and West, K.P., 2005. PMMA: an essential material in medicine and dentistry. *Journal of Long-Term Effects of Medical Implants, 15*(6), pp.629-639.

[6] Bettencourt, A. and Almeida, A.J., 2015. Poly(methyl methacrylate) (PMMA): drug delivery applications. In: Encyclopedia of biomedical polymers and polymeric biomaterials. *Boca Raton: CRC Press*.

[7] Kaur, H. and Thakur, A., 2021. Applications of poly(methyl methacrylate) polymer in dentistry: a review. *Materials Today: Proceedings, 50*, pp.1619-1625.

[8] Dimitrova, M., Corsalini, M., Kazakova, R. et al., 2022. Comparison between conventional PMMA and 3D printed resins for denture bases: a narrative review. *Journal of Composites Science, 6*(3), p.87.

[9] Hashemi, A., Naseri, M., Shahidi, M.M., Mojtabazadeh, H., Salehi, N. and Chireh, M., 2026. Synthesis and investigation of different properties of K_2FeO_4/ZnO and its GO-based nanocomposites. *Progress in Physics of Applied Materials, 6*(1), pp.43-55. DOI: 10.22075/ppam.2025.38094.1151

[10] Treacy, M.M.J., Ebbesen, T.W. and Gibson, J.M., 1996. Exceptionally high Young's modulus observed for individual carbon nanotubes. *Nature, 381*(6584), pp.678-680.

[11] Dresselhaus, M.S., Dresselhaus, G. and Avouris, P. eds., 2001. Carbon nanotubes: synthesis, structure, properties, and applications. *Berlin: Springer*.

[12] Ma, P.C., Siddiqui, N.A., Marom, G. and Kim, J.K., 2010. Dispersion and functionalization of carbon nanotubes for polymer-based nanocomposites: a review. Composites Part A: *Applied Science and Manufacturing, 41*(10), pp.1345-1367.

[13] Singh, R. and Singh, J., 2025. Recent advances in nanostructured cobalt oxide (Co_3O_4): addressing methods and design strategies, challenges, and future directions for non-enzymatic sensor applications. *Sensors and Actuators A: Physical, 387*, p.116404.

[14] Xie, X., Li, Y., Liu, Z.Q. et al., 2012. Nanostructured Co_3O_4 for electrochemical applications. *Small, 8*(14), pp.2201-2217.

[15] Rahmat, M. and Hubert, P., 2011. Carbon nanotube-polymer interactions in nanocomposites: a review. *Composites Science and Technology, 72*(1), pp.72-84.

[16] Bokobza, L., 2007. Multiwall carbon nanotube elastomeric composites: a review. *Polymer, 48*(17), pp.4907-4920.

[17] Kim, S.W., Kim, T., Kim, Y.S. et al., 2012. Surface modifications for the effective dispersion of carbon nanotubes in solvents and polymers. *Carbon, 50*(1), pp.3-33.

[18] Peigney, A., Laurent, C., Flahaut, E. et al., 2001. Specific surface area of carbon nanotubes and bundles of carbon nanotubes. *Carbon, 39*(4), pp.507-514.

[19] ASTM D695-15, 2015. Standard test method for compressive properties of rigid plastics. *West Conshohocken, PA: ASTM International*.

[20] ASTM D2240-15, 2015. Standard test method for rubber property—durometer hardness. *West Conshohocken, PA: ASTM International*.

[21] Cardenas-Flechas, L.J., Barba-Ortega, J.J. and Joya, M.R., 2022. Analysis and evaluation of structural properties of Co_3O_4 microparticles obtained at low temperature. *Ceramica, 68*(385), pp.52-59.

[22] Kumar, A., Pant, M., Mishra, D., Kaur, G., Kumar, D., Kaur, R., Blamah, B.K., Kumar, N., Rustagi, S. and Singh, D., 2026. Sustainable gold nanoparticles possessed significant activity against cancer cell lines (MCF-7, HeLa, and A549). *Progress in Physics of Applied Materials, 6*(2), pp.137-149. DOI: 10.22075/ppam.2025.39282.1175

[23] Zafar, M.S., 2020. Prosthodontic applications of polymethyl methacrylate (PMMA): an update. *Polymers, 12*(10), p.2299.

[24] Coleman, J.N., Khan, U., Blau, W.J. and Gun'ko, Y.K., 2006. Small but strong: a review of the mechanical properties of carbon nanotube-polymer composites. *Carbon, 44*(9), pp.1624-1652.

[25] Tjong, S.C., 2006. Structural and mechanical properties of polymer nanocomposites. *Materials Science and Engineering: R: Reports, 53*(3-4), pp.73-197.

[26] Wetzel, B., Haupert, F. and Zhang, M.Q., 2003. Epoxy nanocomposites with high mechanical and tribological performance. *Composites Science and Technology, 63*(14), pp.2055-2067.

[27] Moniruzzaman, M. and Winey, K.I., 2006. Polymer nanocomposites containing carbon nanotubes. *Macromolecules, 39*(16), pp.5194-5205.

[28] Ahmetli, G., Kocaman, S., Musayev, N., Ozmeral, N. and Isik, M., 2025. Multi-walled carbon nanotubes and graphene oxide-based epoxy hybrid nanocomposites: investigation of nanofiller modification effect. *Surfaces and Interfaces, 72*, p.107265.